The Role of Calcium Hydroxide Precipitation in the Kinetics of Tricalcium Silicate Hydration

Jeffrey W. Bullard

Materials and Construction Research Division,

National Institute of Standards and Technology, Gaithersburg, Maryland USA[*]

Robert J. Flatt

Sika Technology AG, Zürich, Switzerland[†]

(Dated: September 11, 2009)

Abstract

Particles of tricalcium silicate in water typically exhibit a relatively quiescent period (called Stage II) shortly after wetting, lasting up to several hours and during which little apparent reaction occurs. Stage II frequently terminates at about the same time that calcium hydroxide first precipitates from the solution. The close correspondence between these two events led to an early theory that calcium hydroxide precipitation actually triggers a period of accelerating hydration (Stage III), a theory which later gave way to experimental evidence that was thought to contradict it and other theories which were deemed more satisfying from a mechanistic standpoint. This paper surveys several theories and critical experimental data on early-age hydration kinetics of tricalcium silicate. Using HydratiCA, a kinetic cellular automaton model of cement hydration and microstructure development, we investigate two of the leading hypotheses on the mechanism of slow hydration in Stage II, and see for each one the implications of suppressing the growth of calcium hydroxide formation. Each hypothesized mechanism leads to quite different kinetic behavior when calcium hydroxide is suppressed, a result which indicates a line of future experimental inquiry that could decisively determine the Stage II mechanism. Furthermore, the simulations demonstrate how the early theory of calcium hydroxide triggering might be reconciled to the more modern theoretical models and to the experimental data.

[*] jeffrey.bullard@nist.gov

[†] flatt.robert@ch.sika.com

I. INTRODUCTION

This paper addresses the role of portlandite precipitation ($Ca(OH)_2$) on the hydration rate of tricalcium silicate, or alite, the majority mineral phase in portland cement clinker. Hydration of Ca_3SiO_5 (C_3S)[48] progresses through several different kinetic stages, across which the rate of reaction varies nonmonotonically by an order of magnitude or more. Fig. 1 shows these stages generically, but each one can have different duration depending on the conditions of the experiment. Detailed descriptions of each stage are given in several reviews [1–3]. Because this paper investigates particularly the transition from Stage II to Stage III, we will provide here a cursory description of the first three stages, basically following Ref. [3].

In Stage I [49], rapid reactions between C_3S and water occur immediately upon wetting, characterized by a large exothermic signal in isothermal calorimetry experiments [3]. A major contribution to this early exothermic signal is wetting itself, which is characterized by protonation of the oxide ions O^{2-} and SiO_4^{4-} in the C_3S surface structure. Surface protonation is the prerequisite to congruent dissociation of the ion groups into aqueous solution:

$$\begin{aligned} C_3S(3\,Ca^{2+} : O^{2-} : SiO_4^{4}-) + 3\,H_2O \rightarrow \\ (3\,Ca^{2+} : 4\,OH^- : H_2SiO_4^{2}-) \rightleftharpoons 3\,Ca^{2+}_{(aq)} + 4\,OH^-_{(aq)} + H_2SiO_4^{2}-_{(aq)} \end{aligned} \quad (1)$$

The dissociation reaction is initially very fast, up to 10^{-5} mol/m^2/s [3]. However, the reaction decelerates immediately and rapidly as soon as the particles are wet, and reaches a minimum rate within minutes, the beginning of Stage II. At this point, the total calcium concentration in solution is typically about 10 mmol/L, and total silicate concentration is only about 50 μmol/L [4]. Congruent dissolution of C_3S would require a 3:1 molar ratio of calcium to silicon in solution, much lower than observed. To explain the higher Ca/Si ratio in solution, some researchers have proposed incongruent dissolution of C_3S to leave a Si-rich surface layer [4, 5]. But experiments on very dilute suspensions show that dissolution of C_3S is congruent initially, followed by a continual reduction in Ca/Si molar ratio from 3:1 as the dissociation rate decelerates toward Stage II [6]. These latter experiments indicate that the increase in Ca/Si molar ratio in solution is more likely due to the formation of a less-soluble calcium silicate hydrate (C−S−H) phase or phases that have a lower Ca/Si molar ratio than

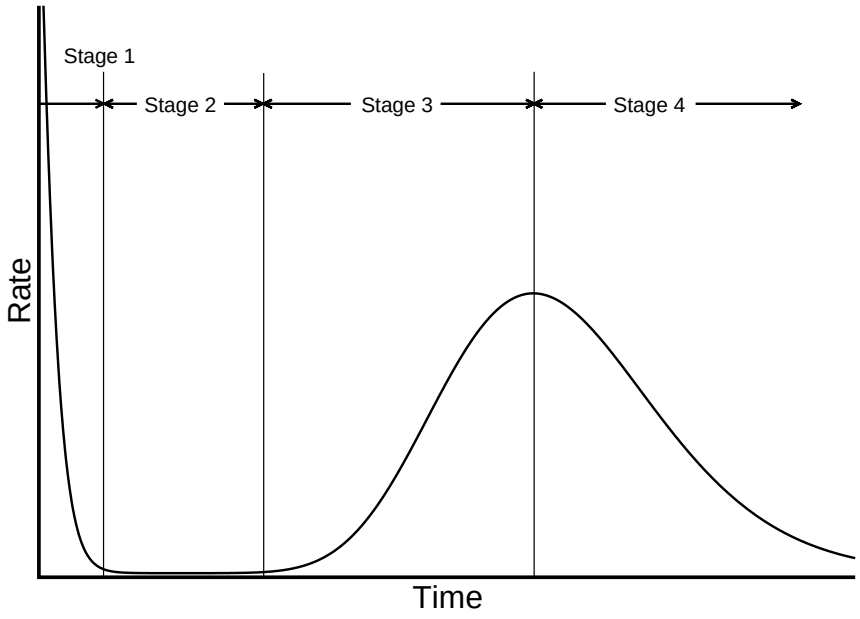

FIG. 1: Idealized rate of hydration of tricalcium silicate as a function of time.

C_3S.

Stage II typically lasts for about an hour or so, after which time a very small amount of C_3S has reacted, less than one per cent. The point of transition to Stage III, the acceleration period, is not well-defined but is characterized generally by a gradual and continuous increase in the rate of hydration which continues until the end of Stage III (see Fig. 1).

The mechanisms of C_3S hydration at early ages have been the subject of some controversy historically, but in recent years a clearer picture has emerged. Carefully controlled experimental studies [7–10] and recent advances in mathematical and computational modeling [11, 12] have contributed to a better understanding of the basic mechanisms that govern the onset and duration of Stage II.

Garrault and Nonat [8, 9] have used a discrete matrix model of anisotropic C−S−H nucleation and growth on C_3S surfaces to fit their experimental measurements of the degree of hydration of C_3S in dilute stirred suspensions in which the concentration of calcium in solution was fixed at either 11 mmol/L or 22 mmol/L, at least until the point of maximum hydration rate within Stage III. Thomas [11] has recently used Cahn's mathematical model of first-order phase transformations at interfaces [13] to show that rate control by nucleation and growth of C−S−H on C_3S surfaces fits experimental isothermal calorimetry measurements of C_3S hydration better than the Avrami-based models which assume that C−S−H

nucleation occurs uniformly throughout the solution volume. Using detailed computer modeling of chemical kinetic mechanisms and microstructure development [12], one of us has shown that rate control by surface nucleation and growth of C−S−H explains the evolution in the solution composition, the Ca/Si molar ratio, and the degree of hydration observed in the studies of Garrault and Nonat as well as an earlier study of C_3S hydration by Kondo and Ueda [14].

General agreement now seems to have been reached that heterogeneously nucleated embryos of C−S−H decorate the surfaces of C_3S particles within seconds or minutes of wetting, and the growth of C−S−H controls the rate of hydration throughout Stages II and III. Initially, the C−S−H surface area available for growth is exceedingly low but increases continuously with more growth. The transition from Stage II to III is actually a continuous increase in the rate of increase in C−S−H surface area and growth rate. But although this mechanistic description of hydration up through Stage III provides a satisfying explanation of the major kinetic features, several questions remain.

A. Why is C_3S dissolution inhibited in Stage II?

Thermodynamic calculations similar to those in Ref. [15] indicate that the solubility product of C_3S should be $K_{sp} \approx 3$ when defined by the net dissociation reaction

$$C_3S + 3\,H_2O \rightleftharpoons 3\,Ca^{2+} + 4\,OH^- + H_2SiO_4^{2-} \tag{2}$$

The calculated K_{sp} is *much* greater, by about 17 orders of magnitude, than the typical ion activity product for Reaction (2) immediately after Stage I [15–17]. Therefore, reduction in the rate of C_3S dissolution would appear to be caused by something other than near equilibrium between C_3S and the solution.

Stein and others have argued that the inhibition is caused by the rapid formation of a continuous but thin metastable layer of C−S−H, called C−S−H(m), that effectively passivates the surface by restricting its access to water in solution, or restricts diffusion of detaching ions away from the surface [16, 18, 19]. This thin layer is proposed to establish near-equilibrium conditions with the solution throughout Stage II. For example, if C−S−H(m) has a composition C_2SH_4 and a net dissociation reaction given by

$$C_2SH_4 \rightleftharpoons 2\,Ca^{2+} + 2\,OH^- + H_2SiO_4^{2-} + 2\,H_2O \tag{3}$$

then solution concentrations during Stage II correspond to an equilibrium constant of $\approx 10^{-11}$ for the hydrate layer. The eventual increase in hydration rates at the end of Stage II is hypothesized to be caused by gradual dissolution of C−S−H(m) in favor of nucleation and growth of a more stable form of C−S−H. The rate of dissolution of C−S−H(m) is controlled by the rate of growth of the more stable C−S−H phase which is responsible for the smooth increase in hydration rates at the end of Stage II.

One of us has recently demonstrated quantitatively how the passivation hypothesis just described can explain a number of experimental observations of the evolution of the solution composition, the composition of the C−S−H products, and the hydration rate of C_3S [12]. That same computer modeling study also showed that the passivation theory is consistent with experimental observations only if nucleation and growth of a stable C−S−H phase also occurs within a few minutes in solutions low in calcium or within an hour in solutions saturated with respect to portlandite. The primary role of the passivating layer in those simulations was therefore to inhibit the dissolution of C_3S until stable precipitates of C−S−H become large enough to control the rate of change in solution composition at the end of Stage II. Throughout this paper, we will refer to this inhibition hypothesis as the *passivation layer hypothesis*.

Other hypotheses about C_3S inhibition have been proposed more recently. One alternative is that C_3S surface protonation causes the subsequent detachment of ions from the surface to be much slower than the initial dissociation rate [6, 20, 21]. A newer hypothesis, well-known in environmental geochemistry [22], is that the molecular mechanism of C_3S dissolution depends on the degree of undersaturation [23]; at large undersaturations, dissolution of some minerals occurs by generation of crystal steps at dislocation etch pits, while at moderate or low undersaturations the driving force is insufficient to activate this mechanism and dissolution occurs by detachment from kink sites along surface steps. This change in mechanism may be augmented by interaction with species already in solution, such as calcium and hydroxyl ions, which could preferentially adsorb and poison the active dissolution sites on the C_3S surfaces [24]. By either of these alternatives, inhibition is caused not by a continuous passivating C−S−H(m) layer, but by a change in the mechanism by which C_3S dissolves. Inhibition therefore could be interpreted as C_3S approaching equilibrium at a much lower "effective" K_{sp}, about 10^{-17} for Reaction (2). To facilitate the discussion that follows, we will refer to this type of inhibition hypothesis—whether by surface protonation,

solute adsorption, or a change in mechanism that deactivtates etch-pit unwinding at lower driving forces—the *site deactivation hypothesis*.

From a practical standpoint, under normal circumstances it may be permissible to pass over the issue of the exact nature of C_3S inhibition in Stage II. For example, Thomas [11] has successfully fit isothermal calorimetry data for alite hydration by assuming only that nucleation and growth of (stable) C−S−H begins at alite surfaces immediately after wetting. However, there are other reasons why better knowledge of the C_3S inhibition mechanism could be important. Knowledge of the mechanism could lead to better understanding of how chemical retarders or accelerators function in cement, or why the efficacy of those admixtures can depend on the time at which they are added to the system. As we show later in this paper, the inhibition mechanism may also significantly affect the way in which portlandite precipitation influences the transition between Stages II and III. Furthermore, we use insights gained from these simulations to propose a line of experimental inquiry that could shed more light on the mechanism that inhibits dissolution of C_3S.

B. How does precipitation of portlandite influence hydration?

At about the same time that hydration begins to accelerate at the end of Stage II, solid $Ca(OH)_2$ is usually observed to precipitate in noticeable quantities [5]. This observation led Young and coworkers to conclude in 1977 that rapid removal of calcium and hydroxyl ions from solution provides the driving force for renewed acceleration of hydration in Stage III. By this mechanism, one might expect that seeding a C_3S suspension with portlandite particles would shorten or eliminate Stage II. However, subsequent experiments of this kind showed no accelerating effect of seeding with $Ca(OH)_2$ particles [25]. Similarly, the use of lime water retards the hydration of C_3S relative to pure water [26]. Furthermore, when Garrault and Nonat hydrated dilute suspensions of C_3S in an aqueous solution in which the calcium concentration was maintained just below the saturation point of portlandite [8, 9], the hydration kinetics followed the typical trends shown in Fig. 1 despite the fact that portlandite could not nucleate in the suspensions. Therefore, the combined experimental evidence after 1977 seemed to indicate that portlandite nucleation cannot trigger the beginning of Stage III.

In this paper, a fundamental computer model of chemical kinetics and microstructure development is used to investigate the transition from Stage II to Stage III. The model

has the advantage that it enables precise control of solute concentrations and local mixing conditions in solution. In addition, it also enables one to prohibit the precipitation of certain minerals regardless of the thermodynamic driving force for their nucleation. These advantages will be used to conduct computer simulations of C_3S hydration under different solution conditions. By comparing the simulation results to published experimental data, a greater insight into the onset of acceleration will be provided and the role of portlandite precipitation will be clarified in a way that reconciles the experimental data that was just surveyed. The computer model is described briefly in the next section before proceeding to the simulations and results.

We should emphasize at the outset, as described more fully in the Results, that we find that both the site deactivation and passivation layer hypotheses can account equally well for existing experimental data on the hydration kinetics of C_3S. This is one of the reasons why we have chosen to examine both options throughout this paper. The other reason is that, as will be shown, suppression of portlandite nucleation has very different implications in both cases. The simulations reported in this paper therefore suggest new ways to differentiate between these hypotheses.

II. MODEL

HydratiCA is a computer model developed recently at the National Institute of Standards and Technology (NIST). Its algorithms are based on fundamental kinetic cellular automaton principles [27]. The details and basic verification of the algorithms are given elsewhere [28, 29]. The material microstructure is discretized on a regular cubic lattice having a lattice spacing of λ. Stoichiometric solid phases (e.g., $Ca(OH)_2$, C_3S), water, and aqueous solute species (e.g, Ca^{2+}, OH^- are defined as separate chemical components. The initial cement particle and water microstructure is mapped onto this lattice by assigning the concentration of each component at each lattice site. For condensed solids, its concentration at a lattice site is equal to its volume fraction there. to each lattice site. These material components are themselves finely discretized into quanta of concentration called *cells*; the number of cells of a given material at a particular lattice point determines its local concentration. This modeling approach has the advantage that the microstructure can be finely resolved both spatially and chemically. The local composition of the solution, for example, can be tracked

at each lattice site to the nearest μmol/L of each component.

Chemical changes and structural development are simulated by iterating over small time increments, each of which is decomposed into independent transport and reaction steps. Diffusion is modeled by allowing each cell at a lattice site to execute a random walk to a neighboring site. The probability p_t of the walk depends on the effective diffusivity D of the mobile species at the site and the length of the time increment τ being considered [28],

$$p_t = \frac{\tau D}{\lambda^2} \tag{4}$$

Similarly, probabilistic rules are formulated to simulate chemical reactions at a lattice site. The probability of occurrence of a given reaction in a time step τ depends on its rate constant and on the number of cells N_α of each reactant α that participates in the reaction [27]:

$$p_{rx}^{(i)} = k\xi^{\left(\sum_\alpha \nu_\alpha^{(i)}\right)-1}\tau \prod_\alpha \max\left[0, \prod_{m=1}^{\nu_\alpha^{(i)}} N_\alpha - m + 1\right] \tag{5}$$

where ξ is a constant model parameter that relates N_α to the molar concentration of species α, and $\nu_\alpha^{(i)}$ is the molar stoichiometric coefficient of the reactant α participating in the reaction. Eq. (5) strictly applies only to homogeneous reactions, i.e. gas phase reactions or solution complexation reactions that can occur uniformly throughout the reaction volume. The same kind of equation applies for heterogeneous reactions, i.e. those that are restricted to interfaces, and nucleation phenomena, although the length scaling is somewhat different [29]. The reaction is allowed if $p_{rx}^{(i)}$ exceeds a random number $q \in [0, 1]$ drawn from a uniform distribution. If the reaction occurs at a lattice site, the number of cells of each reactant (product) is decremented (incremented) by the number required by the molar stoichiometric coefficients of the reaction. By these methods, reactions that can proceed at appreciable rates in both forward and reverse directions can be modeled as two separate one-way reactions, so that equilibrium is characterized as a dynamic balance of the rates of forward and reverse reactions. Consider a reversible reaction between two components A and B to form a third component C:

$$a\mathrm{A} + b\mathrm{B} \underset{k_-}{\overset{k_+}{\rightleftharpoons}} c\mathrm{C}$$

with molar stoichiometric coefficients a, b, and c respectively. If the reaction is elementary, meaning that it involves only one fundamental molecular step, then the rates in the forward

and reverse directions are given by

$$\left.\frac{\mathrm{d}\,[C]}{\mathrm{d}t}\right|_{+} = c\,k_{+}\{A\}^{a}\{B\}^{b}$$
$$\left.\frac{\mathrm{d}\,[C]}{\mathrm{d}t}\right|_{-} = -k_{-}\{C\}^{c}$$

respectively, where square brackets represent molar concentration and curly braces represent activity. The net rate of reaction is found by addition, and is easily shown to be

$$\left.\frac{\mathrm{dC}}{\mathrm{d}t}\right|_{\mathrm{net}} = c\,k_{+}\{A\}^{a}\{B\}^{b}\left(1-\frac{K}{K_{eq}}\right) = c\,k_{+}\{A\}^{a}\{B\}^{b}\,(1-\beta) \tag{6}$$

where $\beta = K/K_{eq}$, often called the saturation index, β, is the ratio of the ion activity product for the reaction, K, to the equilibrium constant K_{eq}. The argument generalizes to any elementary reaction whatsoever. Most reactions of interest in cement hydration are almost certainly not elementary, so there is no guarantee that the form of Eq. (6) is strictly correct [30]. In spite of this, we assume that the reactions modeled here are elementary for several reasons. First, elementary reactions enable a direct connection between the law of mass action and the principle of detailed balances, which provides a convenient tie between each reaction's rate law and its thermodynamic driving force, as described in Ref. [29]. Second, even non-elementary reactions must be composed of a sequence of elementary reactions, each of which will have a net rate equation like Eq. (6), so it is a reasonable "baseline" assumption to use in the absence of conflicting information. Third, the assumption of elementary reactions was tested in a previous paper on modeling C_3S hydration, and it provided good agreement between simulations and a number of experimental observations [12]. Therefore, although most of the reactions we model in this paper are probably not elementary, we do not expect the assumption to cause grave errors for tricalcium silicate simulations. At any rate, the determination of fundamental rate laws for heterogeneous reactions is extremely difficult, especially when several coupled reactions are active simultaneously. Experimental data needed to infer the exact rate laws have not yet been obtained for any of the individual reactions involved in cement hydration. We use the assumption of elementary reactions in the absence of specific contradictory evidence primarily because of its theoretical significance and computational convenience.

Besides the molar stoichiometric coefficients for the reactants and products, each reaction is characterized by its absolute rate constant in either the forward or reverse direction, the

solubility product or equilibrium constant at a reference temperature (taken to be 298 K unless stated otherwise), the activation enthalpy for either the forward or reverse reaction, the enthalpy of reaction, nucleation energy barriers (for heterogeneous reactions only), and stoichiometric coefficients of each reaction. These parameters are sufficient to capture the rate of reaction, the temperature dependence of the rate, and even the temperature dependence of the equilibrium state for reversible reactions [29]. In addition to these reaction parameters, several properties of each of the constituent substances are also required. For simple condensed phases like water and stoichiometric solids, the density, molar volume, and diffusion "transport factor" must be supplied. The transport factor for a phase is defined to be the effective diffusion coefficient of solute through the phase, normalized by the diffusion coefficient in bulk solution. Therefore, the transport factor is a dimensionless number between zero and one, with lower values corresponding to greater resistance to diffusion. For mobile ionic solute species, one must provide the electrical charge, the diffusion coefficient at infinite dilution, and the Kielland ion-size parameters needed to calculate the activity coefficients using the extended Debye-Hückel equation. Values for many of these properties can be found in textbooks or other reference materials [31–34]. Unless stated otherwise, all equilibrium constants, Kielland ion-size parameters, and other thermodynamic data used in this paper are taken from the Nagra/PSI chemical thermodynamic database [35]. Finally, for non-stoichiometric solids like C−S−H, the model simulates compositional and structural variability by microscopic coprecipitation of two stoichiometric end member phases that span the desired range of compositions and physical properties, as described more fully in Ref. [12]. Each end member is assigned values for all the properties just listed, and then the relative rates of formation of each end member at a lattice site determines the local composition of the phase. An similar approach is used in the thermodynamic modeling of non-stoichiometric solids [36].

As this description has implied, all the parameters used in this model have a physical basis and can in principle be checked by independent experiments. However, at this stage the lack of experimental data means that some of the parameter values may need to be adjusted in the future as data become available.

III. MATERIALS AND REACTIONS

Five simulations are described in this paper, designated as simulations A, B, C, D, and E. The conditions for each simulation are summarized in Table I. For simulations A, B, and C, we assume the site deactivation hypothesis for inhibition of C_3S dissolution, which gives C_3S an apparent low solubility product, $\log(K_{sp}^{C_3S}) = -17$. In simulations D and E, however, we assume the passivation layer hypothesis. The hypothesized metastable hydrate, like stable C−S−H, is assumed to have a variable composition with stoichiometric end members denoted by C−S−H(β,m) and C−S−H(γ,m). Table II lists the materials included in all five simulations, along with their assumed properties. The values of density (ρ) and molar volume (v) are taken from published data [32] except for the two assumed stable phases of C−S−H, denoted as C−S−H(β) and C−S−H(γ) following the notation used in Ref. [8]. For these latter phases, values for the average density and molar volume were chosen to be consistent with values reported by in recent publications [37, 38] when the volume of the gel porosity is taken into account. The values for the ionic diffusion coefficients at infinite dilution in water are taken from published thermochemical databases [34]. The actual local diffusion coefficients are calculated from these by including corrections for the concentration dependence of the activity coefficients [28]. The transport factor of each condensed phase in Table II is a dimensionless quantity that, when multiplied by the diffusion coefficient, gives the effective diffusion coefficient for ions diffusing through the internal porosity of the phase. Thus, for water in the absence of any solids, the transport factor is defined to be unity, while for solids with no internal porosity the transport factor is defined to be zero. For solids like C−S−H with nanoscale pores that are not resolved on the scale of the model, a value between zero and one was chosen to estimate the presumably lower rate of transport through these phases.

Table III lists the five reactions that are assumed in simulations A, B, and C. The site deactivation hypothesis is invoked to model the inhibition of C_3S dissolution in Stage II. This assumption stands in contrast to the passivation layer hypothesis which was used in a previous HydratiCA study on C_3S hydration [12].

For simulations D and E, we use the passivation layer hypothesis to inhibit C_3S dissolution, and the assumed rate constants and solubility products are somewhat different than in Table III. For one thing, the passivating mechanism assumes a much more soluble C_3S. In

TABLE I: Summary of simulations performed.

Simulation	**Dissolution Inhibition**	**Solution Conditions**
A	Site deactivation	Pure water initially; solution composition allowed to change naturally
B	Site deactivation	Total calcium concentration fixed at 22 mmol/L throughout simulation; partitioned as $[Ca^{2+}]$ = 18 mmol/L and $[CaOH^{+}]$ = 4 mmol/L
C	Site deactivation	Same as A, except that $Ca(OH)_2$ is not allowed to precipitate
D	Passivation layer	Same as A
E	Passivation layer	Same as C

addition, the solubility products for C−S−H(β) and C−S−H(γ) were modified somewhat from their assumed values in simulations A, B, and C to provide better agreement with published experimental data on solution compositions during Stage II [8, 9]. The dissolution rate constants for C−S−H(β) and C−S−H(γ) also are somewhat different than in Table III, which was necessary to control the rate of dissolution of the metastable layer once the stable forms of C−S−H have nucleated. Table IV summarizes the changes for simulations D and E. Finally, the assumed work of nucleation of C−S−H(β) and C−S−H(γ) are somewhat greater than in simulations A, B, and C, so that the first precipitation of stable C−S−H occurs after about 80 min instead of within the first 10 s.

One additional detail of the simulations is that we make corrections to the dissolution rate constant for C_3S when C−S−H first nucleates and begins to grow on its surface. The correction is required because the initial volume of C−S−H, whether stable or metastable, formed on the C_3S surface is much less than a single lattice site at the surface, so that a surface lattice site will typically still contain bulk solution and C_3S that can react at the initial rate. Partial coverage of the dissolving C_3S surface by a semipermeable C−S−H layer should cause some reduction in dissolution rates, due to cohesive bonding between the layer and the C_3S surface and the restricted access of water molecules to the surface, even when the layer thickness is less than one lattice site. To simulate this reduced dissolution rate, we

TABLE II: List of materials and their assumed properties. The metastable phases C−S−H(β,m) and C−S−H(γ,m) are used only in simulations D and E.

Material/Ion	ρ (kg/m^3)	v (10^{-6} m^3/mol)	Transport Factor, L	$D_\circ$ (10^{-9} m^2/s)
H_2O	1000	18.07	1.0	3.0
C_3S	3210	72.40	0.00	–
C−S−H(β) (CSH_3)	2110	108	0.01	–
C−S−H(γ) (C_2SH_5)	2110	108	0.05	–
C−S−H(β,m) (CSH_3)	2110	108	10^{-4}	–
C−S−H(γ,m) (C_2SH_5)	2110	108	10^{-4}	–
$Ca(OH)_2$	2240	33.08	0.00	–
Ca^{2+}	–	–	–	0.72
OH^-	–	–	–	5.28
$CaOH^+$	–	–	–	0.70
$H_2SiO_4^{2-}$	–	–	–	0.70

TABLE III: List of reactions and their assumed parameters at 298 K for simulations A, B, and C. The fourth reaction is not permitted in simulation C.

Reaction	k_+ (mol/(m$^2\cdot$s))	$\log K_{eq}$
$Ca_3SiO_5 + 3\,H_2O \rightleftharpoons 3\,Ca^{2+} + H_2SiO_4^{2-} + 4\,OH^-$	5.2×10^{-7}	-17.0
C−S−H(β) $\rightleftharpoons Ca^{2+} + H_2SiO_4^{2-} + 3\,H_2O$	1.2×10^{-6}	-7.52
C−S−H(γ) $\rightleftharpoons 2\,Ca^{2+} + H_2SiO_4^{2-} + 2\,OH^- + 5\,H_2O$	1.0×10^{-6}	-12.96
$Ca(OH)_2 \rightleftharpoons Ca^{2+} + 2\,OH^-$	7.19×10^{-6}	-5.20
$CaOH^+ \rightleftharpoons Ca^{2+} + OH^-$	0.06	-1.22

estimate the effective thickness, δ, of the hydration product in the lattice site as its volume divided by the cross-sectional area of the lattice site (1 μm^2 in all the simulations reported here). The rate constant for C_3S dissolution is then decreased linearly with the thickness

TABLE IV: List of reactions and their assumed parameters at 298 K for simulations D and E. The sixth reaction is not permitted in simulation E.

Reaction	k_+ $(\mathrm{mol}/(\mathrm{m}^2 \cdot \mathrm{s}))$	$\log K_{eq}$
$\mathrm{Ca_3SiO_5} + 3\,\mathrm{H_2O} \rightleftharpoons 3\,\mathrm{Ca^{2+}} + \mathrm{H_2SiO_4^{2-}} + 4\,\mathrm{OH^-}$	2.5×10^{-7}	-9.16
$\mathrm{C{-}S{-}H}(\beta) \rightleftharpoons \mathrm{Ca^{2+}} + \mathrm{H_2SiO_4^{2-}} + 3\,\mathrm{H_2O}$	2.2×10^{-7}	-7.52
$\mathrm{C{-}S{-}H}(\gamma) \rightleftharpoons 2\,\mathrm{Ca^{2+}} + \mathrm{H_2SiO_4^{2-}} + 2\,\mathrm{OH^-} + 5\,\mathrm{H_2O}$	6.0×10^{-8}	-12.96
$\mathrm{C{-}S{-}H}(\beta,\mathrm{m}) \rightleftharpoons \mathrm{Ca^{2+}} + \mathrm{H_2SiO_4^{2-}} + 3\,\mathrm{H_2O}$	1.0×10^{-6}	-6.66
$\mathrm{C{-}S{-}H}(\gamma,\mathrm{m}) \rightleftharpoons 2\,\mathrm{Ca^{2+}} + \mathrm{H_2SiO_4^{2-}} + 2\,\mathrm{OH^-} + 5\,\mathrm{H_2O}$	1.6×10^{-7}	-9.92
$\mathrm{Ca(OH)_2} \rightleftharpoons \mathrm{Ca^{2+}} + 2\,\mathrm{OH^-}$	7.19×10^{-6}	-5.20
$\mathrm{CaOH^+} \rightleftharpoons \mathrm{Ca^{2+}} + \mathrm{OH^-}$	0.06	-1.22

according to

$$k_+(\delta) = k_+(0) - \min\left(k_+(0), (1-L)\,\delta\right)$$

where L is the transport factor for the hydration product, shown in Table II. It should be emphasized that this modification only applies while the local effective thickness of the product is less than one lattice site. In the future, this correction could potentially be eliminated by using much finer lattice spacings at the surface through an adaptive meshing technique.

IV. RESULTS

Figure 2 shows the simulated material system, which consists of a single $\mathrm{C_3S}$ particle in solution with a water-cement mass ratio of 0.6. The lattice spacing is $\lambda = 1$ μm, and periodic boundary conditions are used to simulate an infinitely repeated simple cubic array of such particles. The particle is equiaxed with an equivalent spherical diameter of 5 μm. Isosurface rendering was used to produce Fig. 2. As a result, the spatial distribution of phases is accurately reproduced, but the apparent volumes of phases in the image are not quantitatively accurate. The figure shows snapshots of simulation A at 0 min, 120 min and 180 min, when the solution is initially pure water with no control over the solution composition with time. The particle begins dissolving immediately. C−S−H nucleates heterogeneously and

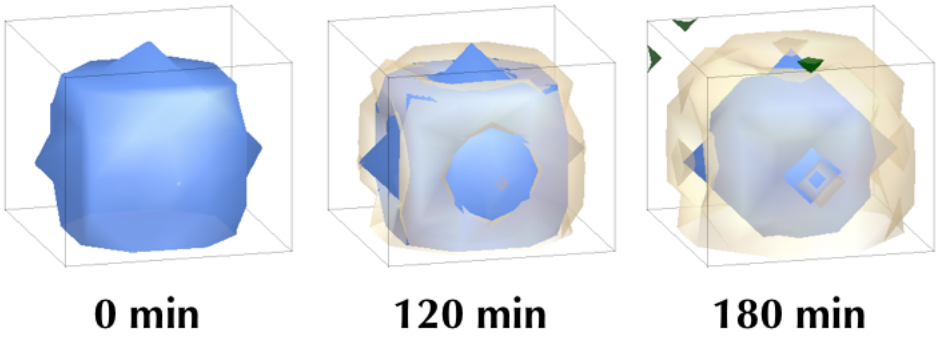

FIG. 2: Material system used in all simulations, consisting of a 5-μm diameter spherical particle of C_3S in solution. The particle initially occupies 34 % of the system volume (w/c = 0.6). The lattice spacing $\lambda = 1$ μm, and periodic boundary conditions are used. Also shown are microstructure after 120 min and 180 min of hydration in pure water with no constraints on the solution composition. The color mapping is blue = C_3S, light brown = C−S−H, dark green = $Ca(OH)_2$.

grows fairly evenly over the entire surface of the C_3S particle. Portlandite (dark green in the figure) nucleates between 1 h and 2 h after hydration, forming some distance away from the particle. These general trends in the microstructure development are consistent with observations reported in the literature (see [3] and references therein).

A. Site deactivation hypothesis

In this section, we present the results from simulations A, B, and C, all three of which use a site deactivation mechanism to model the reduction in C_3S dissolution rate in Stage II. Figure 3 shows the calculated progress of hydration, where we define degree of hydration as the volume fraction of C_3S dissolved, and Figure 4 shows the volume fractions of C−S−H and $Ca(OH)_2$ for all three simulations. Simulations A and B have very similar hydration curves after the first 100 min of hydration, but at earlier times simulation A has greater degree of hydration than simulation B (see inset of Fig. 3).

The early hydration rates of simulation B are lower than simulation A (and C) for two reasons. First, given the higher initial calcium and hydroxyl concentrations, the activity product for C_3S (the first reaction in Table III),

$$K \equiv \{Ca^{2+}\}^3\{OH^-\}^4\{H_2SiO_4^{2-}\}$$

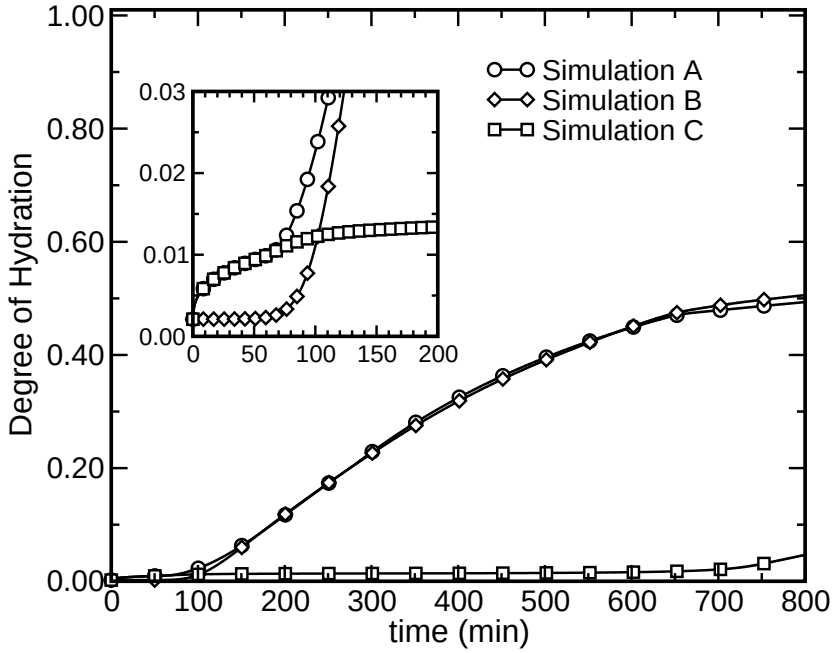

FIG. 3: Degree of hydration as a function of time for simulations A (deact; water), B (deact; fixed [Ca]), and C (deact; no $Ca(OH)_2$).

is nearer to the assumed equilibrium constant of 10^{-17} in simulation B than in simulation A, so C_3S dissolves more slowly in the opening moments of simulation B. Second, the driving force for C−S−H nucleation in the first minute or two is greater in simulation A, which may seem counterintuitive because simulation B starts off with higher calcium and hydroxyl concentrations. Even so, the initial congruent dissolution of C_3S in simulation A is so rapid that the solution quickly reaches greater supersaturation with respect to the low-Ca/Si variant C−S−H(β) in simulation A than it does with respect to either variant in simulation B, where the silicates enter solution more slowly. In fact, C−S−H nucleates and begins to grow within the first ten seconds of hydration in all three simulations, although the volume fractions are so low that this is not resolved in Fig. 4.

Simulations A and B have very similar hydration rates in Fig. 3, despite the fact that $Ca(OH)_2$ does not precipitate in simulation B. In both simulations, C_3S is nearly at equilibrium with the solution. This can be demonstrated by tracking the saturation index, $\beta = K/K_{sp}$, using the concentration of each dissolved component and the extended Debye-Hückel approximation to calculate K as described in Section II. At these solution compositions, the mole fraction of water is greater than 0.995, so Raoult's law is valid for the water

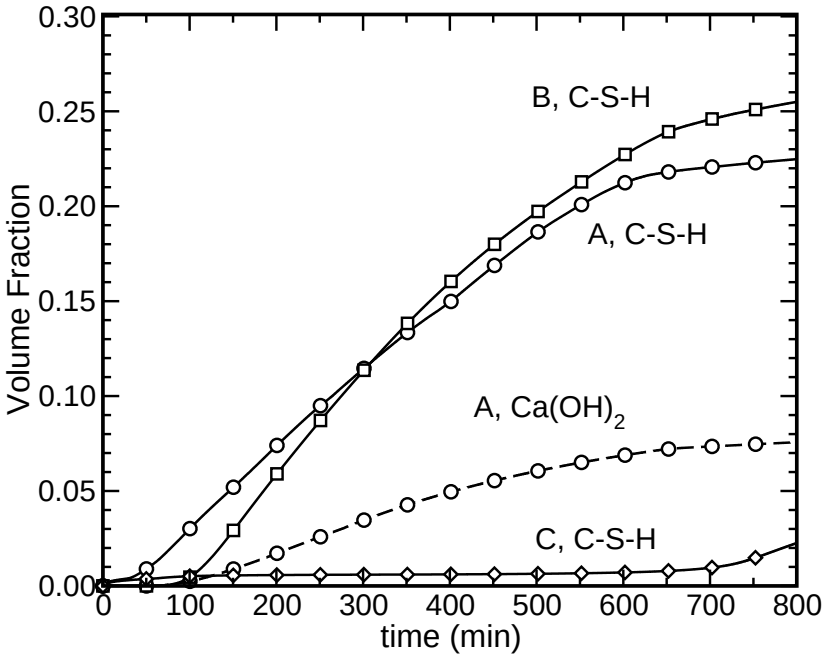

FIG. 4: Time dependence of the C−S−H and $Ca(OH)_2$ volume fractions in simulations A (deact; water), B (deact; fixed [Ca]), and C (deact; no $Ca(OH)_2$).

and we therefore assume that the activity of water is equal to its mole fraction. At 60 min, for example, the calculated values of β for simulations A and B are 0.95 and 0.99, respectively, just slightly undersaturated, for the C_3S dissolution reaction in Table III. Because C_3S is nearly at equilibrium throughout Stage II, we can conclude that hydration rates are controlled by the rate of growth of C−S−H. This conclusion is consistent with previous experimental and modeling results [8, 9, 11, 12], as described in the Introduction.

Not only are simulations A and B similar in Stage II, but they continue to track each other closely throughout Stage III as well. At about 60 min, $Ca(OH)_2$ first nucleates and begins to grow in simulation A, as seen in Fig. 4. As the growing $Ca(OH)_2$ consumes calcium and hydroxyl ions in solution, the concentrations of these two species approaches their values fixed in simulation B. This is shown in Fig. 5, which plots the changes in calcium concentration for all three simulations. Consequently, the solution compositions and volume fractions of solid phases remain very similar in simulations A and B throughout Stage III.

Simulation B is a close approximation to the experimental conditions reported for hydration of C_3S in flow-through reactors [8, 9]. It also closely approximates the experimental conditions when a suspension of C_3S is seeded with small particles of $Ca(OH)_2$; the pres-

ence of solid $Ca(OH)_2$ at the beginning of hydration is a buffering influence that maintains calcium and hydroxyl concentrations very near the $Ca(OH)_2$ saturation point [2, 25, 39]. In agreement with those experiments, simulation B shows only a slight delay in the onset of Stage III (see inset of Fig. 3). Simulation B therefore confirms that the buffering influence of $Ca(OH)_2$ *not* its actual presence in solid form, is responsible for the "normal" hydration behavior observed in simulations A and B. Any other mechanism that could prevent calcium concentrations from increasing much above 20 mmol/L would have the same effect on hydration as solid portlandite.

By themselves, simulations A and B might suggest that $Ca(OH)_2$ precipitation is inconsequential to hydration behavior of C_3S. However, in simulation C, where $Ca(OH)_2$ also is not allowed to precipitate, Stage II lasts about seven times longer than in simulations A and B. Furthermore, it appears that the transition from Stage II to III is less pronounced in simulation C, although some mild acceleration happens near the end of the simulation. An interesting point is that simulations A and C behave identically up to about 60 min of hydration (see the inset to Fig. 3), but then diverge sharply afterward. The divergence happens at the same time as $Ca(OH)_2$ nucleation in simulation A, 60.3 min as shown in Fig. 4, a plot of $Ca(OH)_2$ volume fraction against time for simulation A. Since the only difference between simulations A and C is that $Ca(OH)_2$ cannot form in simulation C, these results imply that strong retardation in simulation C can be caused solely by suppression of $Ca(OH)_2$.

Solution compositions provide supporting evidence for this conclusion. Figures 5 and 6 show the time dependence of the calcium and silicate concentrations, respectively. Just as for their degrees of hydration in Fig. 3, simulations A and C exhibit nearly identical changes in their calcium and silicate concentrations up to about 60 min. Until then, as already demonstrated, C_3S is very near equilibrium with the solution.

In simulation C, the trend of increasing calcium and decreasing silicate concentrations simply continues throughout the rest of the simulation, maintaining near-equilibrium conditions with C_3S and therefore a very low driving force for its dissolution. The inflection in the calcium concentration at 60 min in that simulation is due to the final disappearance of the C−S−H(β) phase, which had been dissolving gradually for many minutes in favor of C−S−H(γ) as the solution evolved to higher Ca/Si ratios. The disappearance of C−S−H(β) adds a degree of freedom to the interactions between the solution, C_3S and

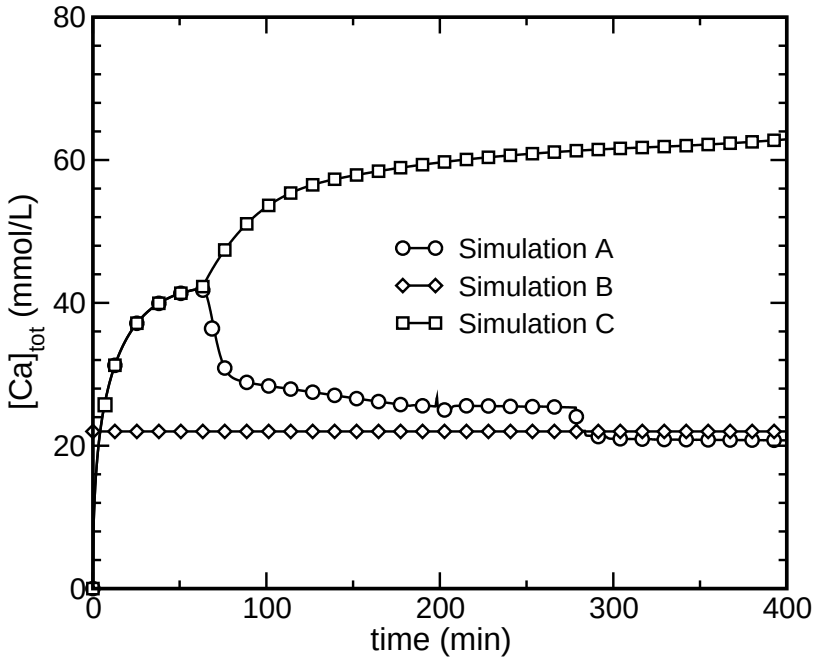

FIG. 5: Total calcium concentration in solution as a function of time for simulations A (deact; water), B (deact; fixed [Ca]), and C (deact; no $Ca(OH)_2$).

C−S−H(γ), causing a relatively rapid increase in calcium concentration. It is a mere coincidence that the disappearance of C−S−H(β) in simulation C occurs at nearly the same time as the nucleation of $Ca(OH)_2$ in simulation A.

The calcium concentration curve is much different in simulation A. Once $Ca(OH)_2$ begins growing at 60 min, it rapidly depletes the dissolved calcium and upsets the C_3S equilibrium. Renewed dissolution of C_3S contributes calcium and silicates to solution, but the calcium continues to be consumed by $Ca(OH)_2$ growth. The net result is an increase in silicate concentration in simulation A from 2 μmol/L to 10 μmol/L within 25 min in Fig. 6, and a corresponding decrease in calcium from 42 mmol/L to 29 mmol/L in Fig. 5. After this rapid readjustment, C_3S is once again only modestly undersaturated, having $\beta = 0.85$. The solution continues to be supersaturated with respect to $Ca(OH)_2$, its saturation index being 2.5. Continued supersaturation with respect to $Ca(OH)_2$ is consistent with experimental observations during Stages II and III [3, 5], and indicates that the growth rate of $Ca(OH)_2$ in this regime is not great enough to reach equilibrium as calcium continues to dissolve from C_3S.

One might intuitively expect the retardation in simulation C to be partially offset by a

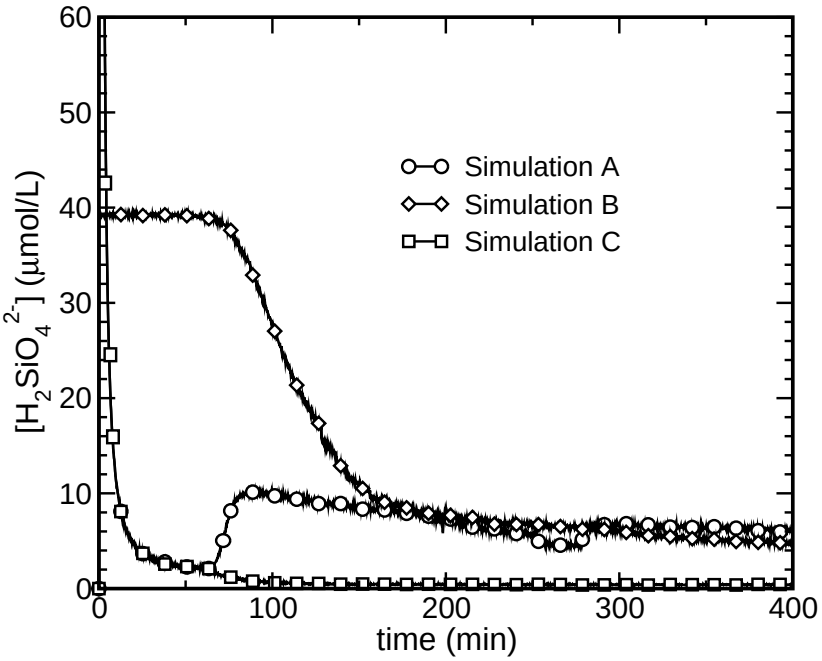

FIG. 6: Silicate concentration in solution as a function of time for simulations A (deact; water), B (deact; fixed [Ca]), and C (deact; no $Ca(OH)_2$).

greater driving force for C−S−H growth, since the concentrations of calcium and hydroxyl ions are greater. We can evaluate this expectation for C−S−H(γ), which is the more stable C−S−H phase in these high-Ca/Si solutions. At 500 min, $\beta = 2.55$ for C−S−H(γ) in simulation A but only 1.32 in simulation C; this means that the thermodynamic driving force for growth of C−S−H(γ) is actually *lower* at later times in simulation C than in simulation A. In effect, the retarding effect of suppressing $Ca(OH)_2$ is further strengthened because it reduces the driving force for growth of the only other hydration product that could upset C_3S equilibrium and stimulate its renewed dissolution.

To summarize, the site deactivation mechanism in Stage II implies that hydration rates should be strongly retarded simply by suppresing $Ca(OH)_2$ formation. It also explains why C_3S hydration is not accelerated either by seeding with $Ca(OH)_2$ particles or by mixing with lime water instead of pure water. Next, we present the results obtained when the passivation layer hypothesis is implemented in HydratiCA.

B. Passivation layer hypothesis

The influence of portlandite precipitation is significantly different in simulations D and E, where a passivating C−S−H(m) layer is invoked to inhibit dissolution of a higher-solubility C_3S phase. Fig. 7 shows the progress of hydration for these two simulations, showing that the transition from Stage II to III is identical for both. In contrast to the previous section, the passivation layer mechanism implies that suppressing $Ca(OH)_2$ formation should have no effect on either the length of Stage II or the initial accelerated rates at the beginning of Stage III. As shown in Fig. 9, precipitation of $Ca(OH)_2$ at about 90 min in simulation D forces the calcium concentration to decrease to about 21 mmol/L, similar to the behavior in simulation A. However, prohibiting $Ca(OH)_2$ (simulation E) enables dissolved calcium to become much more concentrated, 500 mmol/L or greater because the solubility of C_3S is greater. The trends in silicate concentration for simulations D and E, shown in Fig. 10, show the characteristic local minimum in simulation D just before nucleation of $Ca(OH)_2$, followed by a rapid increase and local maximum shortly thereafter. These features are absent when $Ca(OH)_2$ precipitation is not allowed in simulation E, just as for simulation C in the previous section.

The much different effect of $Ca(OH)_2$ precipitation in these simulations, compared to that in simulations A–C, is a consequence of the much greater solubility of C_3S that is assumed in the passivation layer hypothesis. At 125 min, well into Stage III in these simulations, the calculated saturation index for C_3S dissolution in Table IV is $10^{-8.2}$ in simulation D and is $10^{-5.8}$ in simulation E. That is, C_3S is extremely undersaturated at 125 min and the driving force term $(1-\beta)$ in Eq. (6) is basically indistinguishable from unity in both simulations.

Fig. 7 indicates a divergence in hydration rates after about 150 min, with simulation D continuing at about the same rate but simulation E showing a gradual decrease in rate. The rate decrease in simulation E is not due to any significant change in the driving force for C_3S dissolution; its $\beta = 10^{-4}$, and the driving force term $(1-\beta)$ is still basically indistinguishable from unity. Instead, we have traced the rate reduction to re-precipitation of small quantities of the metastable C−S−H(γ,m) phase at the C_3S surfaces. Analysis of the bulk solution composition indicates that it is highly undersaturated with respect to C−S−H(γ,m), having a saturation index of only 0.02. One would therefore not expect it to be stable. However, in lattice sites where C_3S is dissolving, surges in the silicate concentration due to dissolution

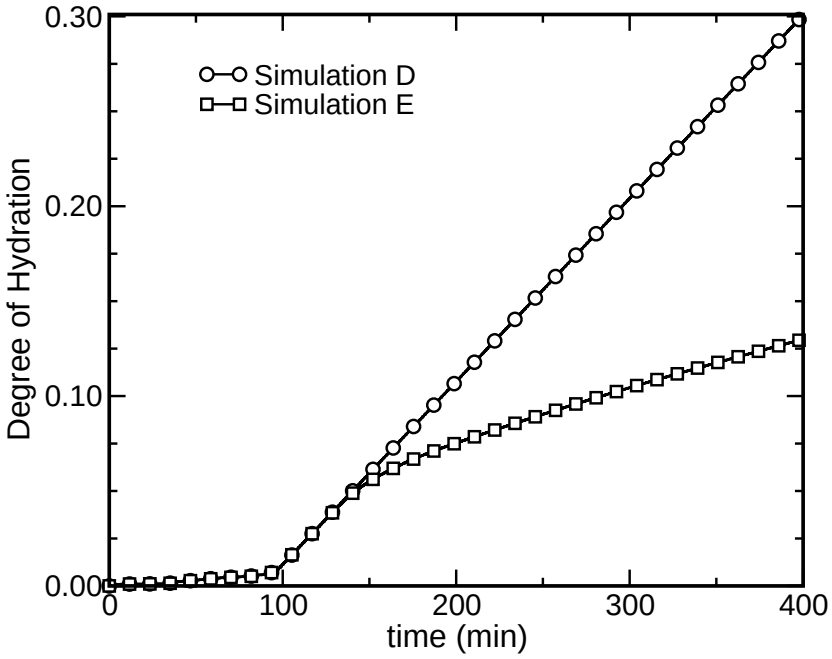

FIG. 7: Degree of hydration as a function of time for simulations D (passivation; water) and E (passivation; no $Ca(OH)_2$).

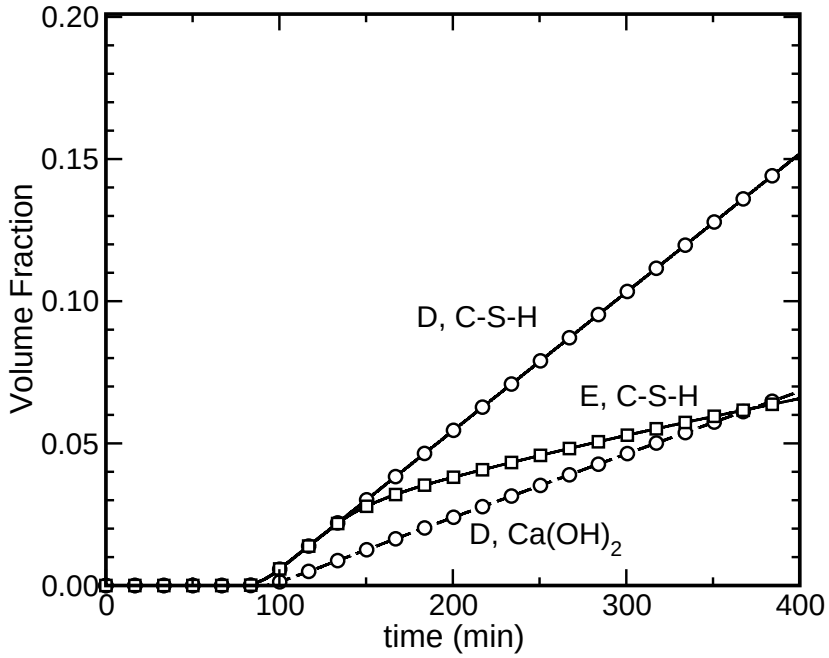

FIG. 8: Time dependence of the volume fractions of C−S−H and $Ca(OH)_2$ in simulations D (passivation; water) and E (passivation; no $Ca(OH)_2$).

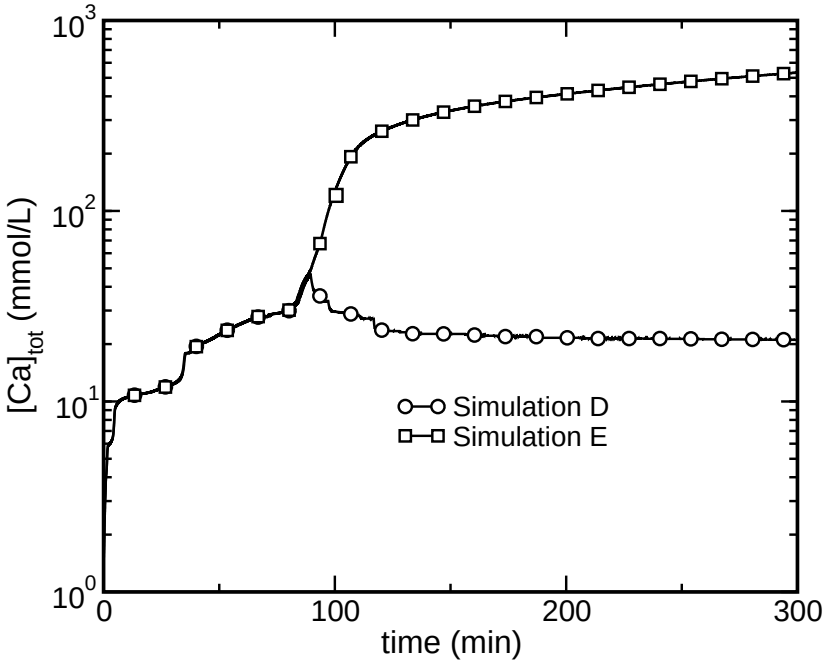

FIG. 9: Time dependence of the total calcium concentration in solution for simulations D (passivation; water) and E (passivation; no $Ca(OH)_2$).

events elevate the local saturation index temporarily, before the silicates can diffuse away from the interface. Even so, the metastable phase is not expected to coexist indefinitely in the presence of the lower-solubility stable C−S−H(γ) phase, so its persistence in simulation E at later times must be the result of its relatively high rate constant allowing it to form quickly before subsequently dissolving in favor of the stable phase. We will have more to say about the later-age behavior of simulation E in the Discussion. For now, the main result of simulations D and E is that suppressing portlandite precipitation should not change the length of Stage II if a passivation layer hypothesis is correct, in marked contrast to the behavior observed when using the site deactivation hypothesis.

V. DISCUSSION

The mechanism for inhibiting C_3S dissolution in Stage II has been controversial for so long because it has been quite difficult to distinguish between them experimentally. Direct observation of a continuous metastable hydrate layer, only tens of nanometers thick, has never been made to our knowledge, but instead has been inferred from particular interpre-

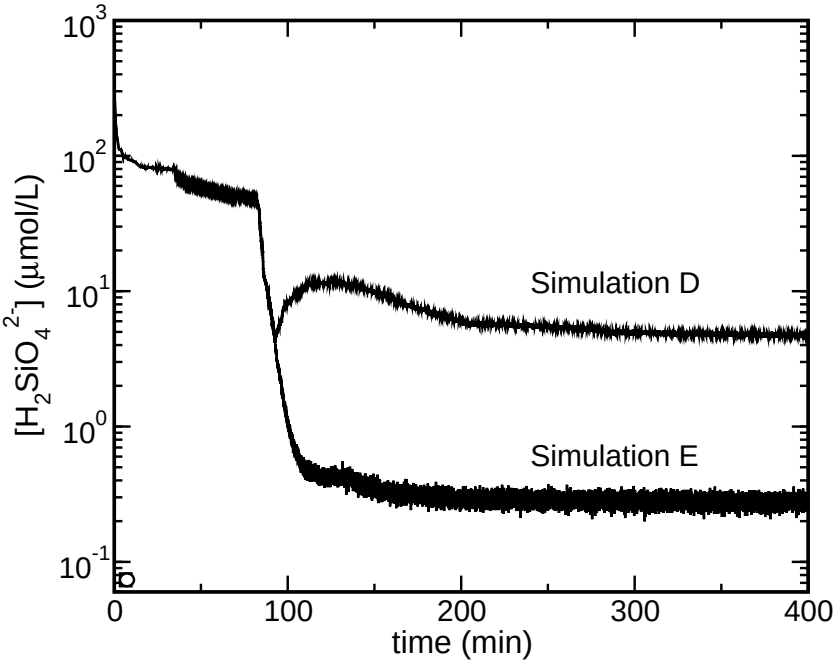

FIG. 10: Time dependence of the silicate concentration in solution for simulations D (passivation; water) and E (passivation; no $Ca(OH)_2$).

tations of solution composition data and thermodynamic analyses [15, 16, 18, 19]. Nuclear resonance reaction analysis indicates that H is incorporated immediately upon wetting the surface of C_3S, and some have taken this to indicate a hydrate layer covering the surface [40], but that interpretation of the data has not been universally accepted. On the other hand, the site deactivation hypothesis, while also able to explain solution concentrations and hydration rates in Stage II, is also difficult to confirm unequivocally. A change in mechanism, from opening of surface defects at high driving forces to step retreat at lower driving forces, has been confirmed for low-solubility minerals like calcite [41], gibbsite [22], and quartz [42], but not for C_3S or other high-solubility minerals. Some investigators have observed surface features of C_3S [43] and Portland cement [44] by scanning electron microscopy in the first minutes of hydration that they interpret as opening of screw dislocation cores or grain boundaries. But direct experimental evidence for this mechanism in cement is sparse, too.

We have intentionally avoided favoring one mechanism over the other in this paper. Instead, we have used HydratiCA to test them both and to see if one or the other might display signature behavior under certain conditions that might be tested experimentally. Our simulations indicate that each mechanism should manifest a significantly different response

in hydration kinetics if $Ca(OH)_2$ precipitation is suppressed, and we have given detailed explanations of the sources of those differences in the Results section. These differences are qualitatively and quantitatively distinct enough that one could imagine the following experiment that could lend critical insight into the mechanism of C_3S inhibition in Stage II. The experiment involves continuously monitoring the hydration rate of C_3S suspended in pure water up through Stage III, and then repeating the experiment using various dosages of a chemical additive that retards $Ca(OH)_2$ growth without noticeably affecting growth or dissolution of any other phases. Continuous measurement of net hydration rates are routinely made by isothermal calorimetry, and if the calorimetric signature were to indicate a strong retardation when $Ca(OH)_2$ is suppressed, it would constitute strong evidence in favor of a site deactivation mechanism. Alternatively, if no significant difference in hydration kinetics were to be observed through Stage III, that would provide strong evidence for the passivation layer mechanism.

The feasibility of such an experiment depends on being able to identify an admixture that selectively adsorbs on $Ca(OH)_2$ surfaces. It would not necessarily need to completely prohibit portlandite nucleation and growth, but it would need to be highly selective in adsorbing only on $Ca(OH)_2$ but not on either C_3S or C−S−H. Sucrose and lignosulfate are known to be strong cement retarders, and there is evidence that their retardation mechanism for C_3S hydration in particular is related to adsorption on, or incorporation into, surfaces of $Ca(OH)_2$ or C−S−H [45, 46], but the data do not enable a determination of how selective the adsorption is. Experiments on suspensions of portlandite alone or C−S−H alone in simulated pore solutions, in which the depletion rate of calcium is measured in the presence or absence of these additives, might help identify a suitable candidate.

If a site deactivation mechanism is responsible for Stage II, the simulations reported here could also reconcile some of the different views on the role of portlandite precipitation in triggering the onset of Stage III hydration. Young's conclusion in 1977 [5] was that $Ca(OH)_2$ precipitation directly causes the transition from Stage-II to Stage-III hydration by depleting the solution of calcium and hydroxyls and thereby renewing C_3S dissolution. Assuming a site deactivation mechanism in Stage II, simulations A and C fully support that conclusion, showing that portlandite precipitation upsets the equilibrium between C_3S and the solution, which leads to renewed dissolution of C_3S and a greater driving force for C−S−H growth than if portlandite formation is suppressed. Experiments where C_3S pastes are seeded with

portlandite particles [25] do not provide meaningful tests of Young's conclusion, as shown by simulation B, because it is not the mere presence of solid portlandite that is important, but the effect that portlandite nucleation has in rapidly changing the solution composition after it is already rich in calcium. This inference from our simulations is in contrast to that drawn in several review papers [1–3] which reject Young's conclusion based primarily on the evidence of those seeding experiments.

In contrast, Young's conclusion is not very plausible if a passivation layer mechanism is responsible for Stage II. Simulations D and E indicate that the duration of Stage II is unaffected by portlandite precipitation because the assumed solubility of C_3S is so great that the driving force for its dissolution is not significantly influenced by the calcium concentration in solution up to a few hundred mmol/L.

On the subject of our simulations of the passivation layer hypothesis, the results of simulation E at later ages, beyond 150 min, should be viewed with caution. After Stage III is well under way in Fig. 7, the calcium and hydroxyl concentrations in solution for simulation E rise to one mol/L or more, corresponding to ionic strengths in excess of 1.5 mol/L. At these high concentrations, the extended Debye-Hückel approximation that we use for calculating activity coefficients is known to be inaccurate [47], so we cannot claim a high quantitative accuracy for the reaction driving forces and rates after 150 min in simulation E. In particular, one should be skeptical of the later-age result in Fig. 7 that metastable C−S−H(γ,m) re-precipitates and passivates C_3S after 150 min in simulation E, causing a shortened Stage III. That possibility must be investigated further, using more accurate estimates of activity coefficients in strong electrolytes, before we can have confidence in it. Persistence of some metastable C−S−H to later ages is consistent with Gartner's views on the role of metastable C−S−H and the passivation layer hypothesis [2], in that he suggests the metastable phase should form so readily on C_3S that it might undergo continual formation and re-dissolution throughout much of early-age hydration. However, this area is especially speculative and we have no direct experimental evidence that the metastable form can persist to these late ages, even if the passivation layer hypothesis itself is valid.

The issues raised here about the origin of Stage II and the possible effects of suppressing portlandite formation could have direct practical implications for the control of portland cement concrete properties at early ages because C_3S is the majority clinker phase and is largely responsible for setting and heat release. More detailed knowledge of the Stage II

mechanism could lead to more rational design of chemical additives for tailoring early-age behavior.

VI. SUMMARY

Kinetic cellular automaton computer simulations have been performed to examine the hydration kinetics of C_3S according to either of two hypotheses for the existence of Stage II: (1) a site deactivation hypothesis by which the type of active dissolution sites C_3S may change with the thermodynamic driving force for dissolution, giving C_3S an apparent solubility that is much lower than the solubility calculated from thermodynamics; (2) a passivation layer hypothesis, by which a low-permeability, metastable hydrate layer forms on the surface of C_3S and restricts its access to water at early ages, but which later dissolves in favor of a more stable hydrate phase.

The simulations indicate that either mechanism can lead to "normal" hydration of C_3S that is typically observed experimentally, in which Stage II lasts for about one or two hours and is followed by a gradual transition to Stage III acceleration. Both mechanisms also lead to changes in solution composition that are consistent with those reported in the literature for C_3S hydration. However, the two mechanisms lead to markedly different behaviors if the precipitation of $Ca(OH)_2$ is suppressed. When a site deactivation mechanism is assumed, suppression of $Ca(OH)_2$ causes a strong retardation, extending Stage II by several hours because low-solubility C_3S is able to remain near equilibrium and because the driving force for C−S−H growth is reduced. In contrast, suppressing $Ca(OH)_2$ formation has no effect on the length of Stage II when a passivation layer mechanism is assumed because (a) the dissolution of the passivating layer is triggered by precipitation of stable C−S−H not $Ca(OH)_2$, and (b) once the passivating layer dissolves, C_3S remains far from equilibrium regardless of whether $Ca(OH)_2$ is present or not.

The results of these simulations suggest experiments that could decisively differentiate between the site deactivation hypothesis and the passivation layer hypothesis for C_3S in Stage II. The feasibility of such experiments depends on identifying an additive that could selectively adsorb on $Ca(OH)_2$ embryos and suppress their growth while not affecting either C_3S or C−S−H surfaces. Further research is probably needed to identify a suitable additive.

Only if a site deactivation mechanism is responsible for Stage II, precipitation of port-

landite can be a direct trigger for Stage III hydration (Young's conclusion), provided that the system is not buffered to limit the concentration of calcium in solution in any other way. This does not imply, however, that adding portlandite seeds to C_3S systems should accelerate hydration, as some have assumed should happen if Young's conclusion is correct. The buffering effect of portlandite seeds ensures that the calcium concentration cannot appreciably exceed saturation with respect to $Ca(OH)_2$. In such a system, or any other system in which the calcium concentration is buffered, hydration rates are controlled by growth of C−S−H throughout Stages II and III, and slow but ever-increasing growth rate of C−S−H in Stage II gradually pulls the solution further and further out of equilibrium with C_3S thereby leading to Stage III as C_3S dissolution is renewed.

Acknowledgments

This work was supported by the Virtual Cement and Concrete Testing Laboratory Consortium and by the Sustainable Concrete Materials program at the National Institute of Standards and Technology.

---

[1] H. F. W. Taylor, P. Barret, P. W. Brown, D. D. Double, G. Frohnsdorff, V. Johansen, D. Ménétrier-Sorrentino, I. Odler, L. J. Parrott, J. M. Pommersheim, M. Regourd, J. F. Young, The hydration of tricalcium silicate, Mater. Structures 17 (1984) 457–468.

[2] E. M. Gartner, J. M. Gaidis, Hydration mechanisms, I, in: J. Skalny (Ed.), Materials Science of Concrete, Vol. 1, American Ceramic Society, Westerville, OH, 1989, pp. 95–125.

[3] E. M. Gartner, J. F. Young, D. A. Damidot, I. Jawed, Hydration of Portland cement, in: J. Bensted, P. Barnes (Eds.), Structure and Performance of Cements, 2nd Edition, Spon Press, New York, 2002, pp. 57–113.

[4] M. E. Tadros, J. Skalny, R. S. Kalyoncu, Early hydration of tricalcium silicate, J. Am. Ceram. Soc. 59 (7–8) (1976) 344–347.

[5] J. F. Young, H. S. Tong, R. L. Berger, Composition of solutions in contact with hydrating tricalcium silicate pastes, J. Am. Ceram. Soc. 60 (5–6) (1977) 193–198.

[6] D. Damidot, A. Nonat, C_3S hydration in dilute and stirred suspensions: (I) study of the two

kinetic steps, Adv. Cem. Res. 6 (21) (1994) 27–35.

[7] D. Damidot, A. Nonat, P. Barret, Kinetics of tricalcium silicate hydration in diluted suspensions by microcalorimetric measurements, J. Am. Ceram. Soc. 73 (11) (1990) 3319–3322.

[8] S. Garrault-Gauffinet, A. Nonat, Experimental investigation of calcium silicate hydrate (C-S-H) nucleation, J. Cryst. Growth 200 (1999) 565–574.

[9] S. Garrault, A. Nonat, Hydrated layer formation on tricalcium and dicalcium silicate surfaces: Experimental study and numerical simulations, Langmuir 17 (2001) 8131–8138.

[10] S. Garrault, T. Behr, A. Nonat, Formation of the C–S–H layer during early hydration of tricalcium silicate grains with different sizes, J. Phys. Chem. B 110 (2006) 270–275.

[11] J. J. Thomas, A new approach to modeling the nucleation and growth kinetics of tricalcium silicate hydration, J. Am. Ceram. Soc. 90 (10) (2008) 3282–3288.

[12] J. W. Bullard, A determination of hydration mechanisms for tricalcium silicate using a kinetic cellular automaton model, J. Am. Ceram. Soc. 91 (7) (2008) 2088–2097, eRB G2008-0142.

[13] J. W. Cahn, The kinetics of grain boundary nucleated reactions, Acta Metall. 4 (1956) 449–459.

[14] R. Kondo, S. Ueda, Kinetics and mechanisms of the hydration of cements, in: Proceedings of the Fifth International Symposium on the Chemistry of Cement, Part II. Hydration of Cements, Vol. 2, 1968, pp. 203–212.

[15] H. N. Stein, Thermodynamic considerations on the hydration mechanisms of Ca_3SiO_5 and $Ca_3Al_2O_6$, Cem. Concr. Res. 2 (2) (1972) 167–177.

[16] E. M. Gartner, H. M. Jennings, Thermodynamics of calcium silicate hydrates and their solutions, J. Am. Ceram. Soc. 80 (10) (1987) 743–749.

[17] A. Nonat (2008).

[18] H. N. Stein, J. M. Stevels, Influence of silica on the hydration of 3 CaO,SiO_2, J. Appl. Chem. 14 (1964) 338–346.

[19] H. M. Jennings, P. L. Pratt, An experimental argument for the existence of a protective membrane surrounding Portland cement during the induction period, Cem. Concr. Res. 9 (1979) 501–506.

[20] P. Barret, D. Ménétrier, Filter dissolution of C_3S as a function of the lime concentration in a limited amount of lime water, Cem. Concr. Res. 10 (1980) 521–534.

[21] P. Barret, D. Ménétrier, D. Bertrandie, Mechanism of C_3S dissolution and problem of the

congruency in the very initial period and later on, Cem. Concr. Res. 13 (1983) 728–738.

[22] A. Lasaga, A. Luttge, Variation of crystal dissolution rate based on a dissolution step wave model, Science 291 (2001) 2400–2404.

[23] P. Juilland, E. Gallucci, R. J. Flatt, K. Scrivener, Dissolution theory applied to the induction period in alite hydration, Cem. Concr. Res.Submitted.

[24] D. Damidot, F. Bellmann, B. Möser, T. Sovoidnich, Calculation of the dissolution rate of tricalcium silicate in several electrolyte compositions, Cement-Wapno-Beton 12/74 (2) (2007) 57–67.

[25] I. Jawed, J. Skalny, Surface phenomena during tricalcium silicate hydration, J. Colloid Interface Sci. 85 (1) (1982) 235–243.

[26] P. W. Brown, C. L. Harner, E. J. Prosen, The effect of inorganic salts on tricalcium silicate hydration, Cem. Concr. Res. 16 (1985) 17–22.

[27] T. Karapiperis, B. Blankleider, Cellular automaton model of reaction-transport processes, Physica D 78 (1994) 30–64.

[28] J. W. Bullard, Approximate rate constants for nonideal diffusion and their application in a stochastic model, J. Phys. Chem. A 111 (11) (2007) 2084–2092, eRB G2006-1935.

[29] J. W. Bullard, A three-dimensional microstructural model of reactions and transport in aqueous mineral systems, Modelling Simulation in Mater. Sci. Eng. 15 (2007) 711–738, eRB G2006-2164.

[30] A. C. Lasaga, Rate laws of chemical reactions, in: A. C. Lasaga, R. J. Kirkpatrick (Eds.), Kinetics of Geochemical Processes, no. 8 in Reviews in Mineralogy, Mineralogical Society of America, 1981, pp. 1–68.

[31] D. Langmuir, Aqueous Environmental Geochemistry, Prentice-Hall, London, England, 1997.

[32] H. F. W. Taylor, Cement Chemistry, 2nd Edition, Thomas Telford, London, 1997.

[33] D. L. Parkhurst, User's guide to PHREEQC—a computer program for speciation reaction-path, advective-transport, and geochemical calculations, Water-Resources Investigations Report 95-4227, U.S. Geological Survey (1995).

[34] R. Mills, V. M. M. Lobo, Self-Diffusion in Electrolyte Solutions, Elsevier, Amsterdam, 1989.

[35] W. Hummel, U. Berner, E. Curti, F. J. Pearson, T. Thoenen, Nagra / PSI Chemical Thermodynamic Data Base 01/01, Universal Publishers, Parkland, Florida, 2002.

[36] B. Lothenbach, F. Winnefeld, Thermodynamic modelling of the hydration of Portland cement,

Cem. Concr. Res. 36 (2006) 209–226.

[37] H. M. Jennings, A model for the microstructure of calcium silicate hydrate in cement paste, Cem. Concr. Res. 30 (2000) 101–116.

[38] A. J. Allen, J. J. Thomas, H. M. Jennings, Composition and density of nanoscale calcium-silicate-hydrate in cement, Nature Mater. 6 (2007) 311–316.

[39] J. M. Gaidis, E. M. Gartner, Hydration mechanisms, II, in: J. Skalny, S. Mindess (Eds.), Materials Science of Concrete, Vol. 2, American Ceramic Society, Westerville, OH, 1989, pp. 9–39.

[40] R. A. Livingston, J. S. Schweitzer, C. Rolfs, H. W. Becker, S. Kubsky, Characterization of the induction period in tricalcium silicate hydration by nuclear resonance reaction analysis, J. Mater. Res. 16 (3) (2001) 687–693.

[41] R. S. Arvidson, I. E. Ertan, J. E. Amonette, A. Luttge, Variation in calcite dissolution rates: A fundamental problem?, Geochimica et Cosmochimica Acta 67 (9) (2003) 1623–1634.

[42] P. M. Dove, N. Han, Kinetics of mineral dissolution and growth as reciprocal microscopic surface processes across chemical driving force, in: AIP Conference Proceedings, Vol. 916, 2007, pp. 215–234.

[43] T. Sakurai, T. Sato, A. Yoshinaga, The effect of minor components on the early hydraulic activity of the major phases of Portland cement clinker, in: Proceedings of the Fifth International Symposium on the Chemistry of Cement, Part II. Hydration of Cements, Vol. 1, 1969, pp. 300–321.

[44] J. M. Makar, G. W. Chan, End of the induction period in ordinary Portland cement as examined by high-resolution scanning electron microscopy, J. Am. Ceram. Soc. 91 (4) (2008) 1292–1299.

[45] N. L. Thomas, J. D. Birchall, The retarding action of sugars on cement hydration, Cem. Concr. Res. 13 (1983) 830–842.

[46] M. Bishop, A. R. Barron, Cement hydration inhibition with sucrose, tartaric acid, and lignosulfate: Analytical and spectoscopic study, Industrial Eng. Chem. Res. 45 (21) (2006) 7042–7049.

[47] H. S. Harned, B. B. Owen, The Physical Chemistry of Electrolytic Solutions, 3rd Edition, Reinhold Publishing, New York, 1958.

[48] Where it is convenient and not likely to cause confusion, conventional cement chemistry notation is used, i.e. C = CaO, S = SiO_2, and H = H_2O.

[49] At least one review [3] divides Stage I into Stages 0 and I, the former being the time before the initial peak in calorimetry curves, and the latter being the time between that peak and Stage II.